Identification of Low Coronal Sources of "Stealth" Coronal Mass Ejections Using New Image Processing Techniques

Alzate, Nathalia; Morgan, Huw

Published in:
Astrophysical Journal

DOI:
10.3847/1538-4357/aa6caa

Publication date:
2017

Citation for published version (APA):
Alzate, N., & Morgan, H. (2017). Identification of Low Coronal Sources of "Stealth" Coronal Mass Ejections Using New Image Processing Techniques. *Astrophysical Journal*, *840*(2), 1-14. [103]. https://doi.org/10.3847/1538-4357/aa6caa

The Astrophysical Journal, 840:103 (14pp), 2017 May 10 https://doi.org/10.3847/1538-4357/aa6caa

Identification of Low Coronal Sources of "Stealth" Coronal Mass Ejections Using New Image Processing Techniques

Nathalia Alzate and Huw Morgan
Institute of Mathematics, Physics and Computer Science Prifysgol Aberystwyth Ceredigion, Cymru SY23 3BZ, UK; naa19@aber.ac.uk
Received 2016 November 11; revised 2017 April 4; accepted 2017 April 10; published 2017 May 12

Abstract

Coronal mass ejections (CMEs) are generally associated with low coronal signatures (LCSs), such as flares, filament eruptions, extreme ultraviolet (EUV) waves, or jets. A number of recent studies have reported the existence of stealth CMEs as events without LCSs, possibly due to observational limitations. Our study focuses on a set of 40 stealth CMEs identified from a study by D'Huys et al. New image processing techniques are applied to high-cadence, multi-instrument sets of images spanning the onset and propagation time of each of these CMEs to search for possible LCSs. Twenty-three of these events are identified as small, low-mass, unstructured blobs or puffs, often occurring in the aftermath of a large CME, but associated with LCSs such as small flares, jets, or filament eruptions. Of the larger CMEs, seven are associated with jets and eight with filament eruptions. Several of these filament eruptions are different from the standard model of an erupting filament/flux tube in that they are eruptions of large, faint flux tubes that seem to exist at large heights for a long time prior to their slow eruption. For two of these events, we see an eruption in Large Angle Spectrometric Coronagraph C2 images and the consequent changes at the bottom edge of the eruption in EUV images. All 40 events in our study are associated with some form of LCS. We conclude that stealth CMEs arise from observational and processing limitations.

Key words: Sun: activity – Sun: corona – Sun: coronal mass ejections (CMEs) – Sun: filaments, prominences – Sun: flares

Supporting material: animations

1. Introduction

Coronal mass ejections (CMEs) are generally associated with eruptive phenomena or low coronal signatures (LCSs) in the lower corona such as solar flares, filament eruptions, extreme ultraviolet (EUV) waves, magnetic reconfiguration, or jets. Eruptions apparently lacking LCSs have been observed as early as the 1970s and 1980s (Howard & Harrison 2013) and have continued to be a topic of interest. A study by Robbrecht et al. (2009b) gave rise to the term "stealth" CMEs, where they refer to events lacking on-disk signatures as "problem storms." Many subsequent studies of these events provide different interpretations of "stealth" CMEs (e.g., Ma et al. 2010; Kilpua et al. 2014).

Robbrecht et al. (2009b) described a slow CME with no clear indication of a filament eruption or flare preceding it, observed by white light coronagraphs during 2008 June 2. Using data from the Extreme Ultraviolet Imager (EUVI) and images from the COR1 and COR2 coronagraphs on board *Solar TErrestrial RElations Observatory* (*STEREO*)/Sun Earth Connection Coronal and Heliospheric Investigation (SECCHI, Howard et al. 2008), they concluded that the CME originated in a streamer at a relatively large height. The event was a very slow-rising flux tube that led to a streamer blowout CME (Sheeley et al. 1982; Howard et al. 1985). In their study, EUVI B images did not reveal an LCS, but EUVI A images did reveal a bright structure moving outward to form the core of the CME.

The term "stealth CME" was used by Ma et al. (2010) to describe CMEs without LCSs. Their study focused on 34 CMEs that occurred between 2009 January 1 and August 31. Of these 34 events, 11 were classified as stealth events with velocities $<300\,\mathrm{km\,s^{-1}}$. Through visual inspection of EUVI data, they looked for LCSs for each event. Of the 11 stealth events, 3 revealed no off-limb coronal structures while the other 8 had some structures high in the corona, possibly parts of flux ropes.

Howard & Harrison (2013) state that limitations in instruments and observations may lead to the identification of CMEs as stealth events. Wang et al. (2011) describe a "stealth" CME as one that lacks eruptive signatures in EUV pass-bands and is not always visible in coronagraphs if the CME is Earth-directed. In their study of source locations for 1078 CMEs between 1997 and 1998, about 16% of these events were assumed to be front-sided and lacked eruptive signatures.

Kilpua et al. (2014) identified 10 stealth CMEs in their study of 20 interplanetary CMEs observed in 2009 and found that they lacked the leading bright front in coronagraph images. By their definition, stealth CMEs also lack on-disk and on-limb EUV signatures. They identified these events by searching for large-scale signatures such as EUV dimmings the size of an active region (AR) or larger, erupting prominences with material moving out of the field of view (FOV), post-eruption arcades, and ejection-like limb signatures.

A search for LCSs of post-CME blobs in current sheets, seen in the Large Angle Spectrometric Coronagraph (LASCO, Brueckner et al. 1995) was recently carried out by Schanche et al. (2016). They studied nine events in which a total of 23 blobs were tracked and characterized by an average speed of $<307\,\mathrm{km\,s^{-1}}$. Their analysis of EUV data did not reveal any corresponding signatures for the blobs.

A study by D'Huys et al. (2014) defined a stealth CME as a "front-sided CME that was detected in coronagraph images and for which no coronal signature was observed on the solar disk or in the more extended FOV of EUV imagers." In their work, they assembled a catalog of 40 stealth CMEs observed by LASCO in 2012 and analyzed the observational and kinematic

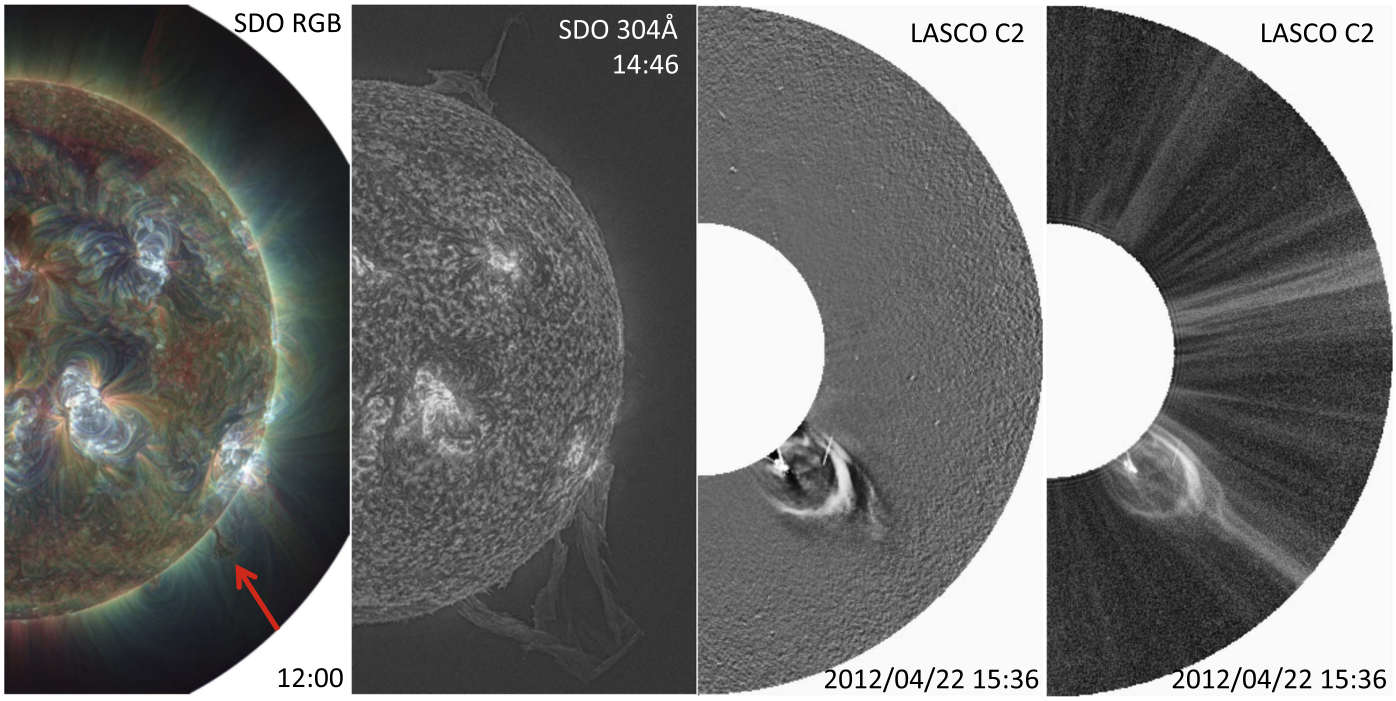

Figure 1. Example of images produced when (left two panels) *SDO*/AIA data are processed with the MGN technique (Morgan & Druckmüller 2014) and (right two panels) LASCO data are processed using the DST (Morgan et al. 2012) and the NRGF (Morgan et al. 2006). The LASCO C2 images reveal a CME in the southwest region caused by a filament eruption (seen in the *SDO* images). The *SDO* RGB image shows a filament (indicated by the arrow) at 12:00 UT, while the 304 Å image reveals the filament when it expands through the FOV and leaves it at around 14:46 UT. The *SDO* RGB image is a superposition of three wavelengths produced using *SDO* 171, 193, and 211 Å.

properties of these events for comparison with those of regular CMEs. They developed a procedure that eliminates obvious non-stealth CMEs. In 2012, CACTus (Robbrecht & Berghmans 2004; Robbrecht et al. 2009a) detected 1596 CMEs in the LASCO images. Using the *Geostationary Operational Environmental Satellite* X-ray Sensor (*GOES*/XRS, Hanser & Sellers 1996) event lists, they filtered out 680 CMEs associated with X-ray flares, at most 4000 s before they were detected by CACTus. Next, D'Huys et al. (2014) compared the CACTus LASCO CME catalog with the CACTus CME detections in SECCHI/COR2 coronagraph images to exclude back-sided CMEs–CMEs that move away from Earth—having a principal angle between 180° and 360°. A total of 809 back-sided CMEs were identified. The next step in their search for stealth CMEs was to compare the CACTus LASCO list to the output of the Solar Flare Automated Search Tool (Bonte et al. 2013), which is based on observations from the Sun Watcher using Active Pixel System detector and Image Processing (SWAP) instrument on board Projects for Onboard Autonomy (PROBA2, Halain et al. 2013; Seaton et al. 2013), in order to eliminate events associated with EUV variability. They found 322 such events. Each of the steps described was carried out independently. Any CME from the CACTus LASCO catalog associated with detections in the other data sets was removed from the list of potential stealth CMEs. This resulted in a list of 481 CMEs without an automatic link to an LCS. After visual inspection of images from observations by PROBA2/SWAP, *STEREO*/SECCHI, and the Atmospheric Imaging Assembly (AIA, Lemen et al. 2012) on board the *Solar Dynamics Observatory (SDO)*, they eliminated CMEs that were associated with filament eruptions, EUV waves or dimmings, or eruptive signatures at larger heights, thus yielding 40 CMEs to analyze.

The aim of our study is to apply advanced image processing methods to properly search for the LCSs of CMEs that have been previously identified as stealth CMEs. As such, we start with, and build upon, the extensive study of D'Huys et al. (2014). New image processing techniques are applied to EUV (Morgan et al. 2012) and white light coronagraph data (Morgan et al. 2006; Morgan & Druckmüller 2014) to reveal the fainter details of coronal dynamics. In our work, we focus on the 40 stealth CME events identified by D'Huys et al. (2014) due to the availability of *SDO* data. Application of new processing methods to these data enable us to investigate the possible existence of observable LCSs. Section 2 describes the main set of instruments and processing methods used in this study. Section 3 describes our data and results in detail, providing our best interpretation of the events in this study. Section 4 summarizes our findings.

2. Instruments and Methods

In this study, we made use of several instruments.

1. The LASCO C2 instrument on board the *Solar and Heliospheric Observatory* (Brueckner et al. 1995) satellite, which acquires white light coronagraph observations. It has a useful FOV spanning 2.2–6.0 $R_{\odot}$, and a spatial resolution of 11.4 arcsec pixel^{-1}. During the observational period presented, the cadence of LASCO C2 was ∼12 minutes.
2. The *SDO*/AIA instrument, which images the solar atmosphere in seven EUV channels and three ultraviolet (UV) visible channels. For this study, only images in the 171 and 304 Å channels were used with a reduced selected cadence of ∼2 minutes. The AIA 171 Å channel images are dominated by emission from Fe IX ions with a

Table 1
Description of the 2012 Events

Event	Date	Angle[5]	Time (UT)*	LASCO C2**	Speed (km s^{-1})[6]	*SDO* 171 Å	*SDO* 304 Å	EUVI (B) 304 Å
1	Jan 7	30	15:24	Blobs	346	Filament eruption	Filament eruption	Filament eruption
2	Jan 7	3	23:48	Blobs	375	Jets	Jets	Jets
3	Jan 19	357	22:36	[1]Blobs	519	Jets	Jets	Jets
4	Jan 20	334	00:24	Blobs	296	Filament eruption	Filament eruption	Filament eruption
5	Jan 20	341	17:12	Blobs	433	Filament eruption	Filament eruption	Filament eruption
6	Jan 26	20	16:38	CME	240	Filament eruption	Filament eruption	Filament eruption
7	Jan 28	311	04:12	[2]Blobs	575	[a]Flares	[a]Flares	Filament eruption
8	Feb 4	357	09:24	CME	130	Jets	Jets	Jets
9	Feb 22	20	12:48	[3]CME	51	Filament eruption	Filament eruption	Filament eruption
10	Feb 22	9	23:48	[3]CME	122	Jets	Jets	Jets
11	Feb 23	45	12:24	[1]Puffs	187	Filament eruption	Filament eruption	Jets
12	Feb 29	16	19:48	CME	113	Filament eruption	Filament eruption	Filament eruption
13	Mar 21	168	23:12	CME	142	Jets	Jets	Jets
14	Apr 19	176	01:36	[1]Puffs	115	Jets	Jets	Jets
15	May 16	179	03:24	CME	173	Jets	Jets	Jets
16	Jun 3	345	07:12	CME	168	Filament eruption	Filament eruption	Filament eruption
17	Jun 9	27	07:24	Blobs	335	Filament eruption	Filament eruption	Filament eruption
18	Jun 17	83	04:48	Blobs	177	[b]Filament eruption	[e]Flares	[e]Flares
19	Jul 7	100	18:00	[4]CME	156	[b]Filament eruption	[a]Flares	[a]Flares
20	Jul 13	330	05:05	[1]Puffs	231	Filament eruption	Filament eruption	Filament eruption
21	Jul 14	334	19:24	Blobs	269	Filament eruption	Filament eruption	Filament eruption
22	Jul 17	318	23:24	Blobs	369	Jets	Jets	Jets
23	Jul 21	76	02:36	Puff	460	[c]Spray	[c]Spray	Jets
24	Jul 28	338	14:24	[1]Blobs	228	Filament eruption	Filament eruption	Filament eruption
25	Aug 12	338	20:24	CME	60	Filament eruption	Filament eruption	Filament eruption
26	Aug 16	40	05:00	CME	110	Jets	Jets	[d]Jets
27	Sep 4	344	03:48	[1]Puff	313	Filament eruption	[d]Filament eruption	[d]Filament eruption
28	Sep 18	3	02:12	[1]CME	363	[d]Filament eruption	[d]Filament eruption	Jets
29	Sep 22	178	07:00	Puffs	316	Jets	Jets	Jets
30	Oct 20	15	23:48	CME	66	Filament eruption	Filament eruption	Filament eruption
31	Oct 28	115	01:48	[1]Blobs	244	Filament eruption	Filament eruption	[b]Filament eruption
32	Nov 3	346	23:24	Blobs	207	Filament eruption	[d]Filament eruption	Filament eruption
33	Nov 14	242	00:00	CME	101	Filament eruption	[d]Filament eruption	Filament eruption
34	Nov 16	353	13:36	[1]Blobs	339	Filament eruption	[d]Filament eruption	[d]Filament eruption
35	Nov 25	24	18:36	CME	64	Filament eruption	Filament eruption	Filament eruption
36	Dec 17	156	03:36	CME	166	Jets	Jets	[d]Filament eruption
37	Dec 18	334	08:24	Puff	232	[d]Filament eruption	[d]Filament eruption	[d]Filament eruption
38	Dec 18	340	18:36	Puff	150	Jets	Jets	[d]Filament eruption
39	Dec 19	350	18:36	Puff	257	Jets	Jets	[d]Filament eruption
40	Dec 20	12	21:17	CME	259	Jets	Jets	[d]Filament eruption

Note. The LCSs associated with the events in LASCO are given for *SDO* 171 and 304 Å and for EUVI B 304 Å. LASCO: [1]aftermath of large CME(s); [2]energetic particle storm; [3]part/edge of a CME; [4]narrow CME. EUV: [a]flares in active region (AR) in conjunction with "sympathetic" filament eruptions (FE); [b]FE(s) near AR; [c]spray(s) following jets; [d]jets near FE; [e]jets and small flares present; [5]principle angle from D'Huys et al. (2014); [6]calculated speeds (bootstrapping); *start time from D'Huys et al. (2014); **DST-processed LASCO data.

peak formation temperature of ∼0.6 MK, and the 304 Å channel is dominated by He II ions at $\sim 5 \times 10^4$ K.

3. The *STEREO*/EUVI instrument, which studies the evolution of the corona in three dimensions. The EUV imagers on board *STEREO* provide an additional perspective on the activity in the low corona. For this study, images with a cadence of ∼5 minutes in the 304 Å channel were used. The 171 Å images were not used due to noise.
4. The COR2 instruments, which are twin coronagraphs on board *STEREO A* and *B* moving in the plane of the ecliptic with different viewing conditions. In 2012, the two spacecraft were aligned on the far side of the Sun from Earth and the separation angle between them decreased from 142° on January 1 to 100° on December 31. Their FOV is ∼3–14 $R_\odot$ and thus enables a view of each event from the back side of the Sun. COR1 images, with an FOV from 1.5 to 4 $R_\odot$, are too noisy to show much detail.
5. The PROBA2/SWAP instrument, which can observe the Sun to larger heights than AIA and EUVI. It observes the Sun in the 174 Å channel with a cadence of ∼1 minute. Due to the lower resolution of SWAP images, applying our processing techniques (see Section 2.1) resulted in much lower quality images than those from AIA and EUVI. Additionally, due to the movement of the instrument, combining images to reduce the signal-to-noise ratio proved futile. However, when possible, we used SWAP images for events that were seen close to the edge of the FOV of AIA and EUVI.

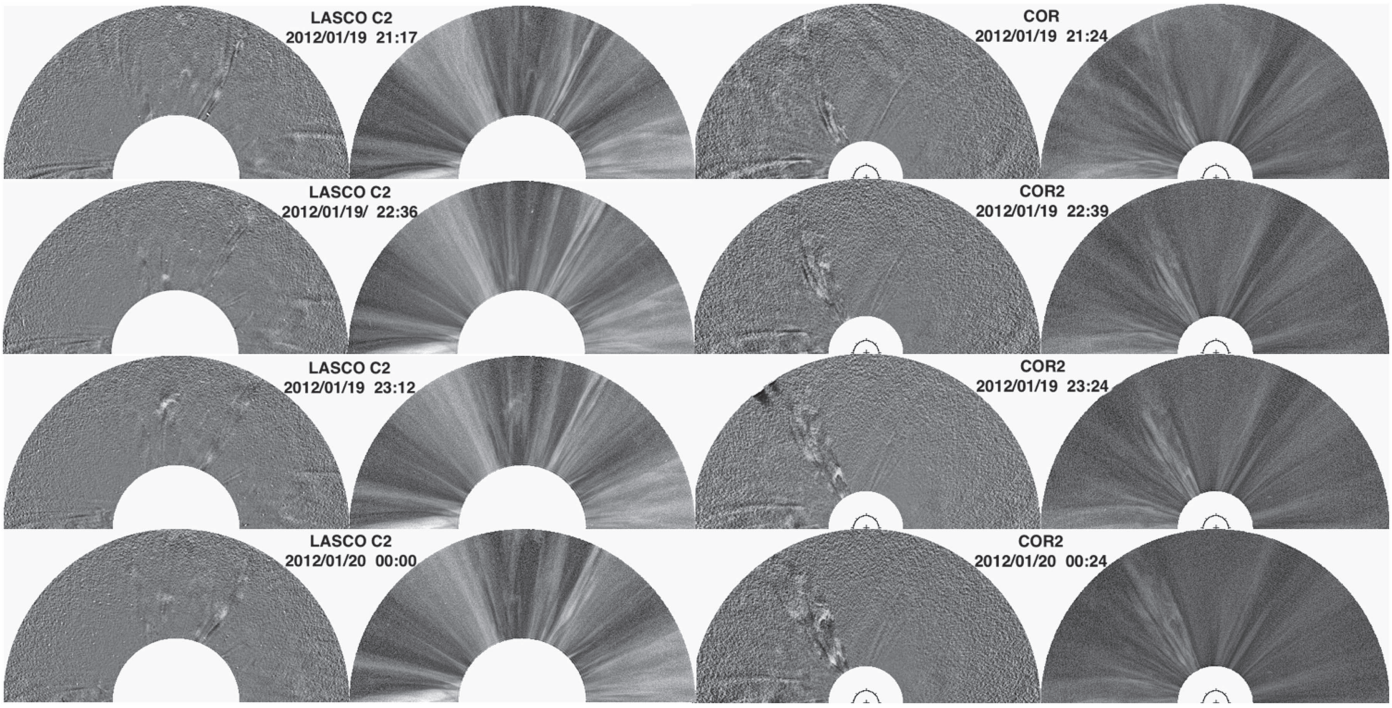

Figure 2. DST-processed LASCO C2 (left) and *STEREO*/COR2 (right) dynamic and original images of the northern region. These images show the course of propagation of a series of blobs from 2012 February 19 beginning around 21:00 UT until 2012 February 20 around 00:00 UT. The back side of this event is seen in *STEREO A*.

2.1. Image Processing Methods

The aim of our study was to apply advanced image processing methods in order to reveal the LCSs of CMEs studied by D'Huys et al. (2014). LASCO C2 images were processed with the Dynamic Separation Technique (DST, Morgan et al. 2012; Morgan 2015), which uses a spatial-temporal deconvolution method to separate the dynamic and quiescent components of the observation. The DST is used to better reveal the faint dynamic events, and gives superior results compared to simpler running- or base-difference methods. The Normalizing Radial Graded Filter (NRGF, Morgan et al. 2006) is a simple filter applied to coronagraph data for removing the steep radial gradient of brightness in the images to better reveal structure. Images that are striking in detail are produced after applying this method. Reliable image processing techniques play an important role in studying coronal events in detail because of the large dynamic range in coronal observations.

EUV images were processed using the Multiscale Gaussian Normalization technique (MGN, Morgan & Druckmüller 2014). This technique aims at revealing information that is often hidden in the broad brightness range of EUV images. It normalizes an image by using the local mean and standard deviation calculated using a Gaussian-weighted sample of local pixels. The normalized image is transformed by the arctan function and this process is applied over several spatial scales. The final image is a weighted combination of the normalized components, plus the original gamma-transformed image, which reveals fine details in the corona and structures in off-limb regions.

When only an elementary level of image processing is applied to coronal imaging observations, many important structural or dynamical details remain hidden. In studies of CMEs in coronagraph data, details are often obscured by quiescent coronal features such as coronal streamers. Figure 1 is an example of our MGN-, NRGF-, and DST-processed images. The processed EUV images (left two panels) clearly reveal the detail of a large filament eruption that is the source of the CME in the coronagraph images (right two panels). In the coronagraph images, the quiescent background is removed, thus isolating the dynamic component (the CME).

2.2. LCS Identification Approach

The purpose of this study was not to analyze individual events in detail, but to identify LCSs. For this reason, only the instrument channels with the highest emission signal were used (i.e., 171 and 193 Å). Additionally, we used the 304 Å channel, which peaks at a lower temperature and reveals cooler material.

The stealth CMEs identified by D'Huys et al. (2014) are detected by CACTus (Robbrecht & Berghmans 2004; Robbrecht et al. 2009a), which is an automated detection software based on difference images from LASCO data. In their paper, the authors provide the time frame during which the CMEs are seen in the LASCO C2 FOV as well as the principle angle, angular width, and velocity for each event. We used their times and angles to identify each event in our DST-processed LASCO C2 data set. These parameters are listed in Table 1. The velocities listed were calculated using the bootstrapping method described in Section 3.2.

The next step in our analysis of the 40 events involved processing the corresponding EUV data using the image processing techniques described in Section 2.1. *SDO*/AIA 171 Å data were processed in two-minute frames to analyze changes in the structure of the corona before each event in LASCO and *SDO*/AIA 304 Å data, also in two-minute frames, were processed and used to identify cooler structures such as prominences. In case some or all of the 40 events in our study had an LCS visible from the backside of the Sun, we also

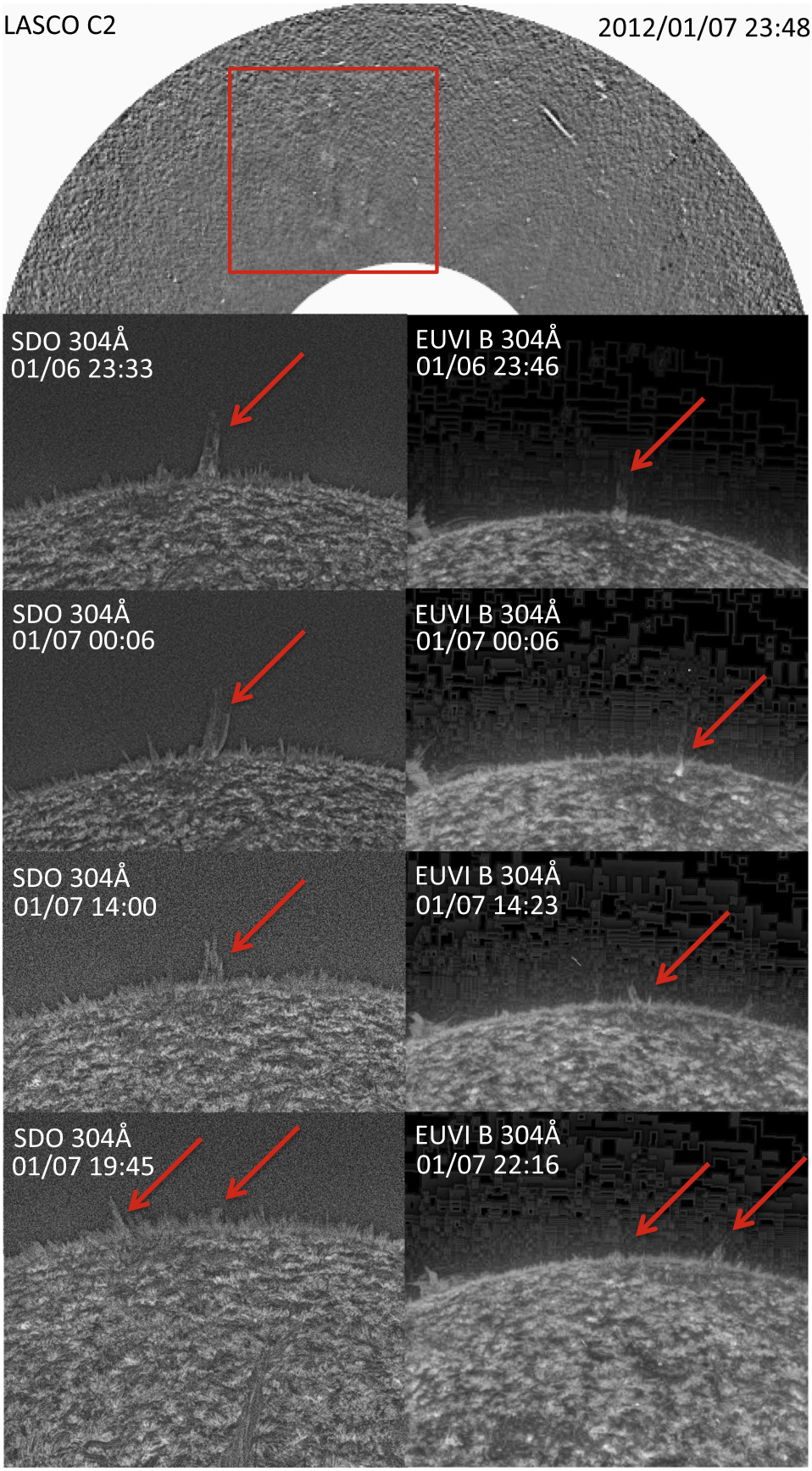

Figure 3. Time series of low coronal signatures for the January 7 event. Top: blob seen in LASCO C2. EUV images (left): jets are the sources of this event seen in *SDO* 304 Å. EUV images (right): the back side of these jets are seen in EUVI B 304 Å images. A small bright eruption is seen at 00:06 UT on January 7 in EUVI B before the next jet.

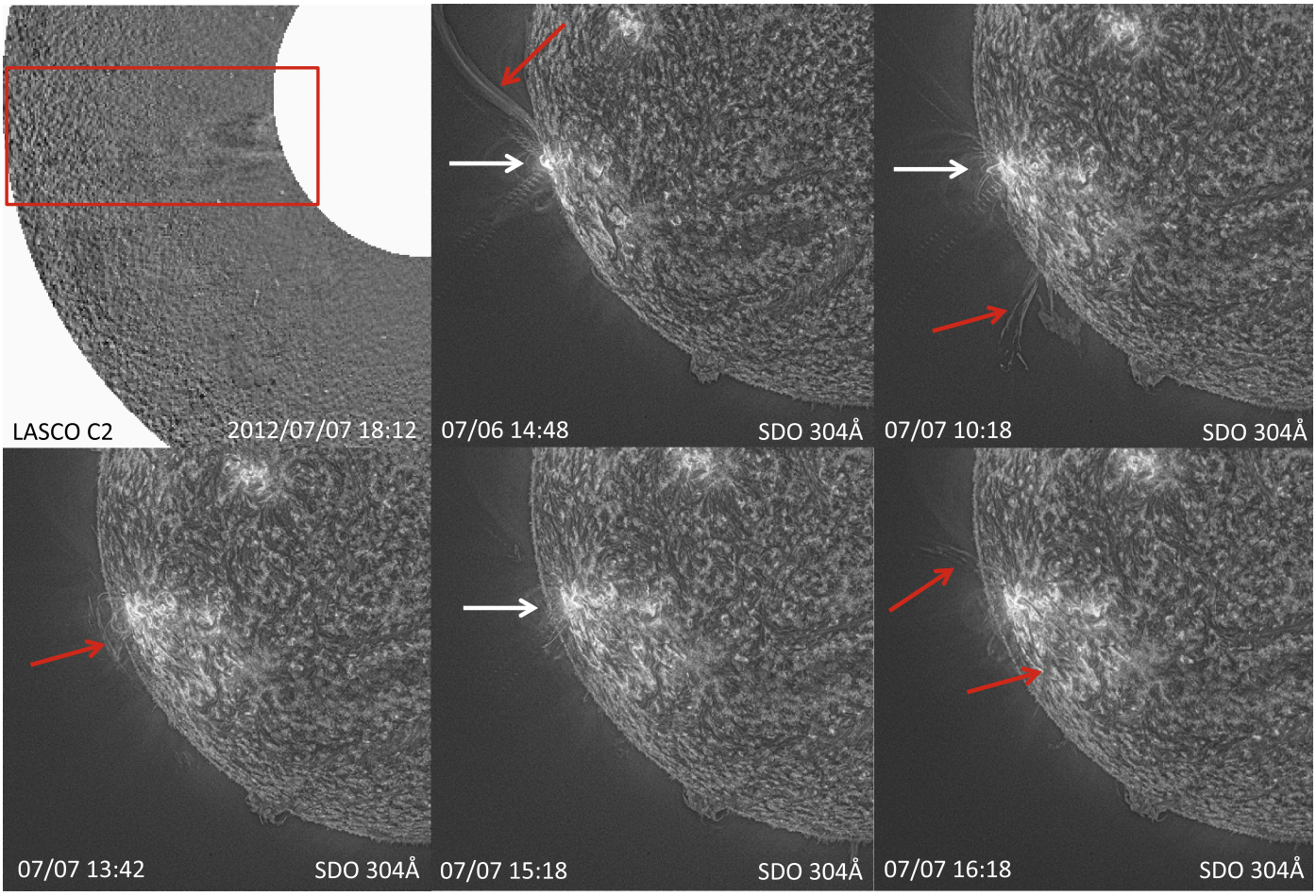

Figure 4. 2012 July 7 CME event moves in the FOV of LASCO C2 beginning around 18:00 UT. EUV images: a close-up of the source region of this event in *SDO* 304 Å. A series of flares began on July 6 and continued throughout July 7 leading up to the time of the event in LASCO C2. The movie in the online version of the journal shows these flares and other eruptions in and around the active region shown. Several "sympathetic" eruptions of filaments are seen in conjunction with the flares.

(An animation of this figure is available.)

processed *STEREO*/EUVI 304 Å data for six-minute frames. SWAP data were also processed for events that had a faint LCS or were visible high in the AIA FOV. However, the detail in the AIA data was superior to SWAP images due to its higher resolution. We identified a subset of EUV data according to the timing and location of each CME.

3. Data Analysis and Results

We undertook a comprehensive manual inspection of all 40 stealth CME events studied by D'Huys et al. (2014), as given in Table 1. With the application of both DST and NRGF image processing techniques to the LASCO C2 data, it became clear that not all of them were typical CMEs. Twenty-three events were classified as unstructured blobs or puffs, often associated with the aftermath of large CMEs. Our classification of these events, based on the processed LASCO C2 data is given in Table 1. As shown by Alzate & Morgan (2016), puffs are fast and faint events that appear to have little structure except for a broad, faint front. They do not possess a classic three-part CME structure: a bright leading front, a cavity, and a bright central core (Chen 2011; Vourlidas et al. 2013). The series of rapid puffs described in Alzate & Morgan (2016) were detected in white light coronagraph data and associated with a series of recurrent fast events or jets. The puffs are likely disturbances caused by an initial reconnection event, propagating along an expanding region of open flux adjacent to a large AR. The puffs do not have an obvious flux rope structure—they are just a broad, faint front of enhanced brightness.

Blobs are narrow flux tubes, or the motion of plasma packets along field lines. The blobs are believed to be a result of magnetic reconnection in current sheets (see Schanche et al. 2016 and references therein). In our study, we see either blobs or puffs in the aftermath of CMEs, but we also see blobs or puffs as isolated events. The blobs shown in Figure 2 are seen in the northern region in the LASCO C2 FOV beginning on 2012 January 19. The COR2 images provide a view of the backside of the blobs in which the structure, or shape, is the same. While it is difficult to make unambiguous associations between small-scale eruptions and frequent small-scale events occurring in EUV images, it is possible to associate all of these blobs (and similarly, puffs) with jets and/or small flares, or a series of jets/small flares arising from a single region, similar to the case study of Alzate & Morgan (2016). Details are provided in Table 1.

Each event in our study exhibited some form of LCS at or above the surface of the Sun, within the FOV of *SDO*. Additionally, 10 events in our study exhibited more than one LCS (see Table 1 for details) in the same region or in the

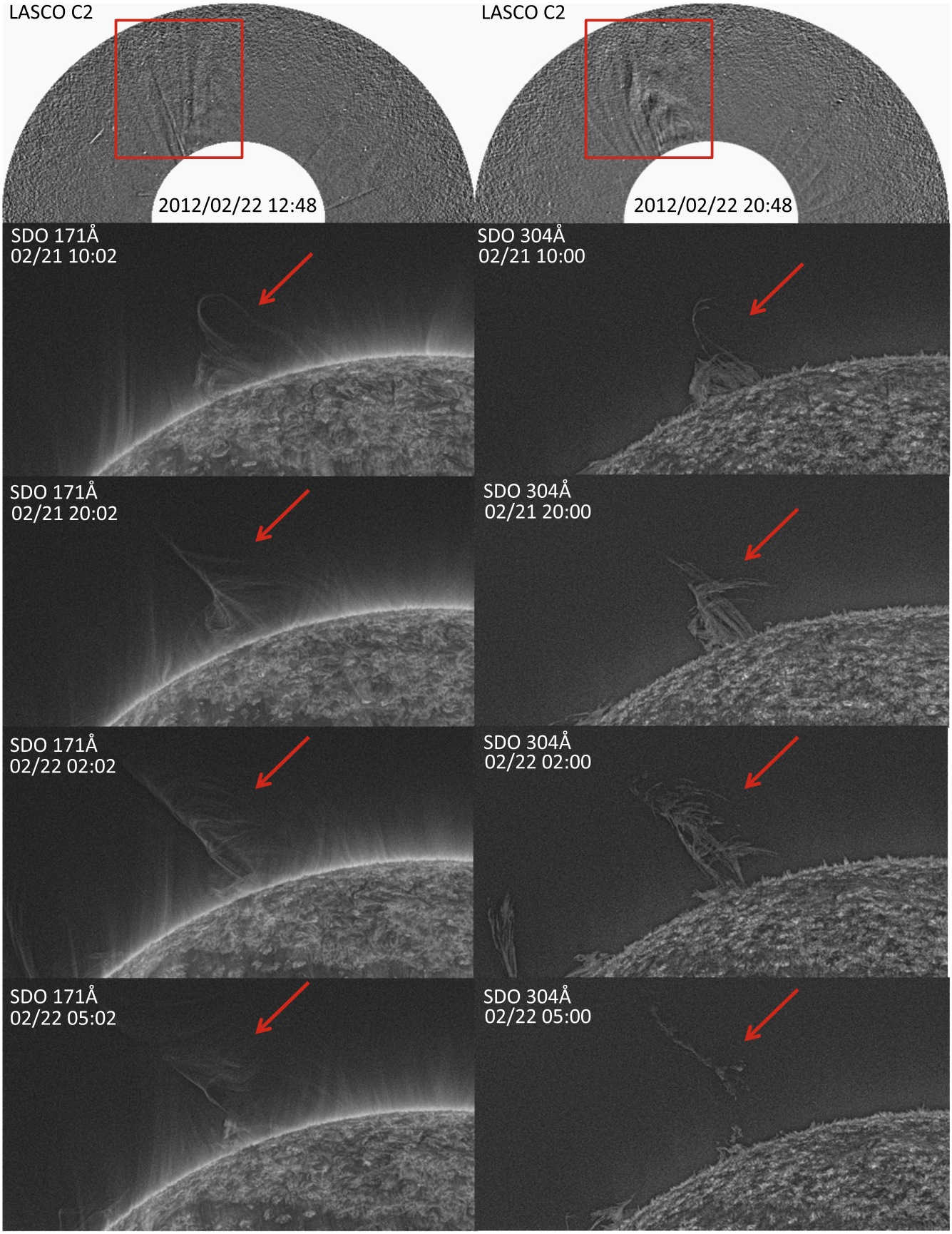

Figure 5. Event 9 was seen in the LASCO C2 FOV beginning at 12:48 UT on February 22 (top left) and expanded through the FOV at 20:48 UT (top right). The filament eruption associated with this event is clearly seen in the subsequent EUV images (left: *SDO* 171 Å, right: *SDO* 304 Å).

(An animation of this figure is available.)

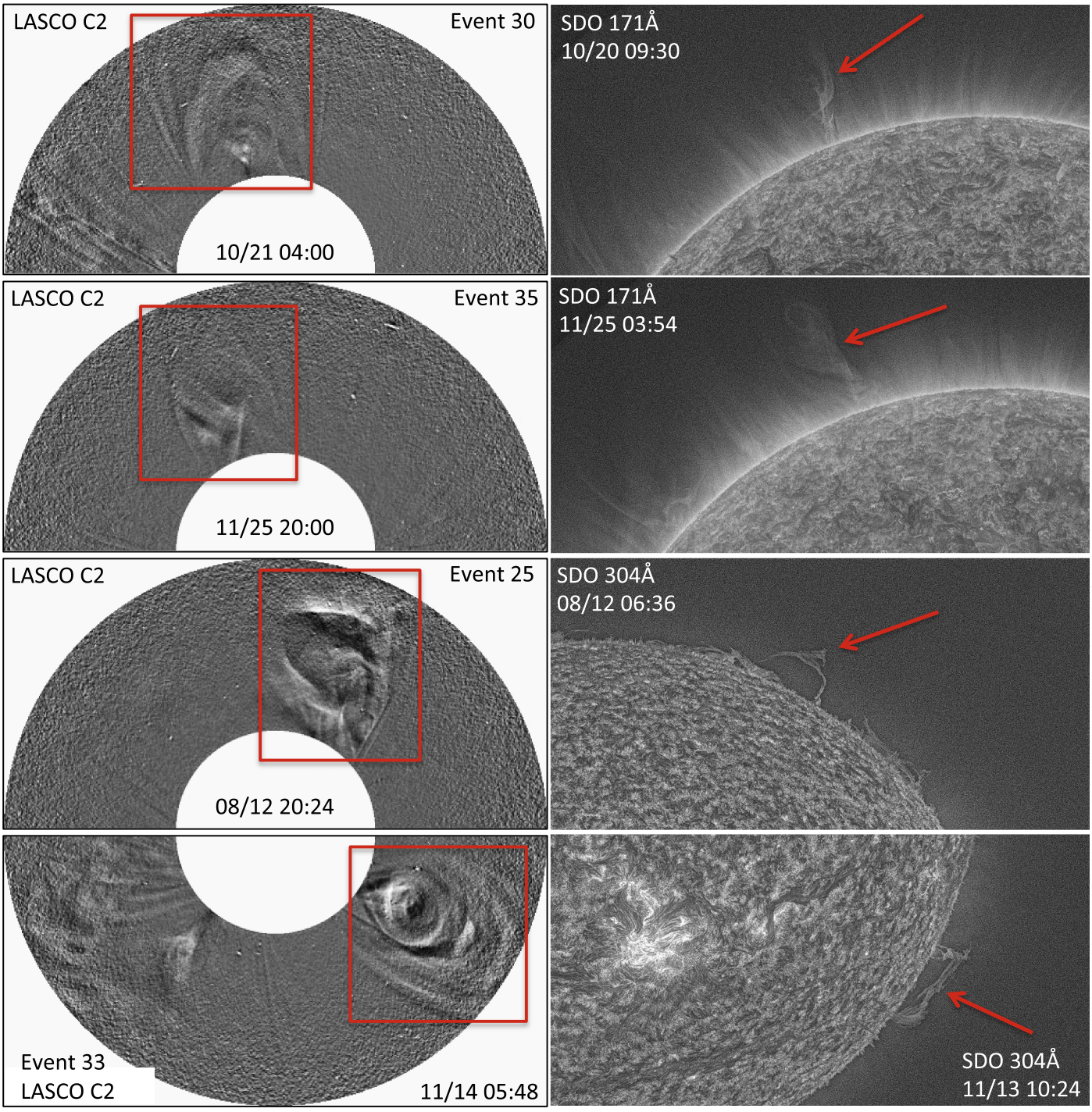

Figure 6. Events 30, 35, 25, and 33 seen in LASCO C2 (left column) and their associated low coronal signatures in EUV (right column).

vicinity (e.g., jets near filament eruptions). It is therefore difficult to be 100% certain of small-scale LCS events being linked to a certain CME. However, based on our findings, we can say with certainty that there is some LCS present for each event presented here. It follows then that these events cannot be labeled as stealth. Because the image processing techniques we used are so effective at revealing fine details in the corona, we found LCSs for all 40 events. Based on our findings, we can summarize these LCSs as follows.

1. 14 events are associated with jets.
2. 1 event is associated with a jet followed by a surge spray.
3. 3 events are associated with a series of flares.
4. 22 events are associated with eruptions or partial eruptions of filaments.

Jets are rapid collimated eruptions of material that are guided through the corona. In this study, we found 14 events associated with jets, most of which led to the blobs and/or puffs described above. Figure 3 shows a series of jets associated with the January 7 event, which entered the LASCO C2 FOV at approximately 23:48 UT and left the FOV on January 8 at 01:12 UT. During this time frame, several blobs were observed crossing the FOV. In the corresponding EUV

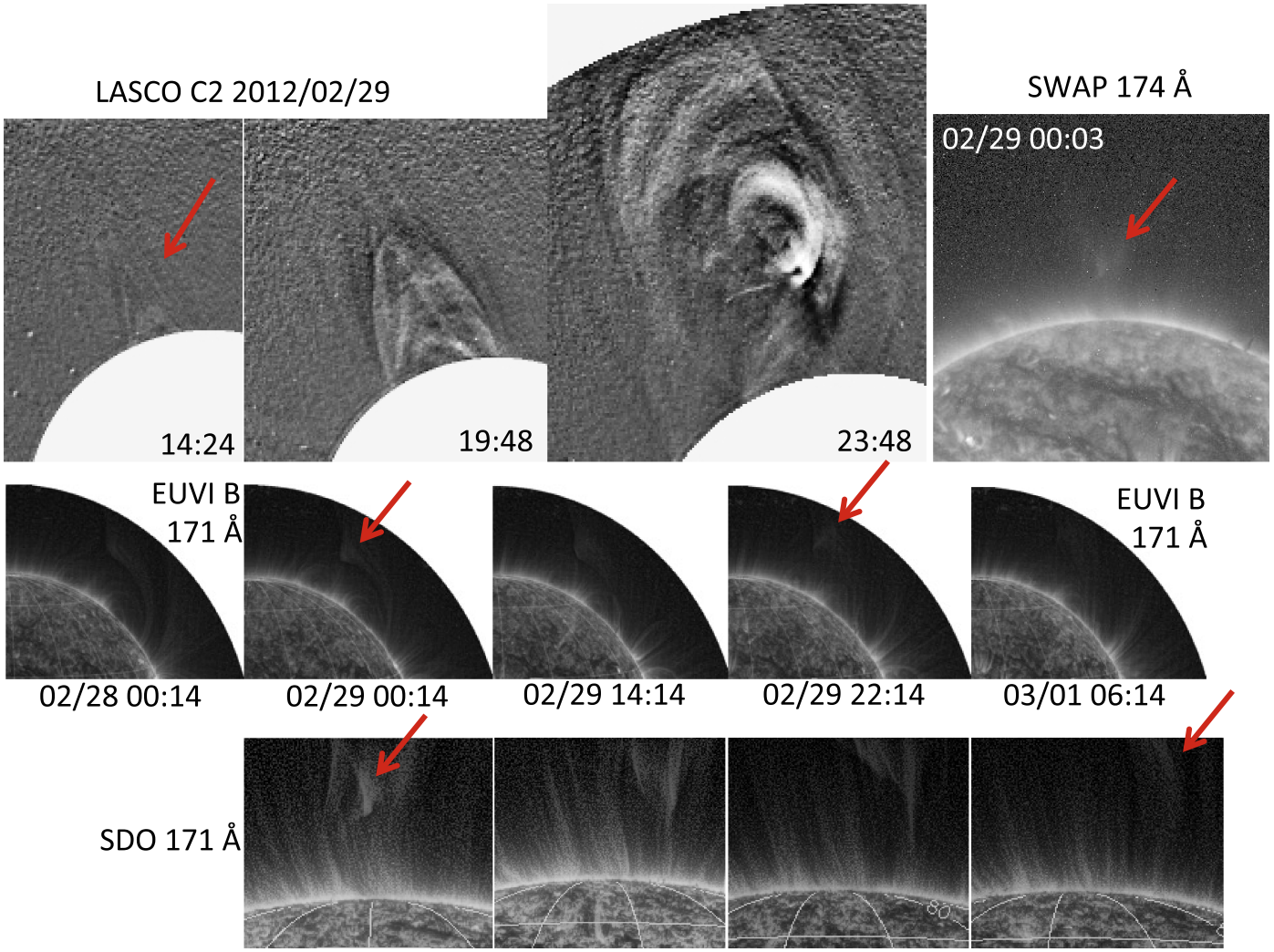

Figure 7. February 29 event (event 12) seen in LASCO C2 around 19:00 UT (top row). The structure that leads to the CME is a wispy structure at large height seen in EUVI B 171 Å (middle row) from its side and in *SDO* 171 Å (bottom row). The structure is also seen in SWAP 174 Å (top right).

images, jet eruptions began on January 6 and continued throughout January 7.

Another event seen in LASCO on July 21 (a puff) was associated with a jet followed by a spray of material. In the 304 Å *SDO* images, the spray begins right after the jet erupts as a secondary eruption (see Alzate & Morgan 2016). It then rises and widens some time later. This was the only LASCO event in this study that exhibited this behavior in the low corona.

Solar flares are sudden flashes of brightness observed near the Sun's surface. Of the 40 events in this study, 3 were associated with a series of flares, 2 of which were also associated with filament eruptions. Figure 4 is an example of a flaring active region with filament eruptions, which led to a narrow CME in LASCO seen on July 7 beginning at 18:00 UT. The velocity for this CME is 156 km s^{-1}. The EUV images show an active region, typically associated with bright spots and arcs of solar material in the Sun's atmosphere, clearly seen along with eruptions at different times. The flares are indicated by white arrows and other activity with red arrows. What makes this event so interesting is that there were many "sympathetic" filament eruptions—eruptions that occurred consecutively widely separated in conjunction with the flares. To fully appreciate this, an *SDO* animation is provided in the online version of Figure 4. Based on the velocity, the activity in the low corona associated with the CME should occur approximately 4.5 hr before the onset of the event in LASCO. At 13:24 UT (bottom left panel), there is some material off limb, partially from a flare (seen in the top right panel indicated by the white arrow) and partially from a filament that erupted just below this region (seen in the top right panel indicated by the red arrow). The bottom middle panel shows another flare approximately 3 hr before the CME. The bottom right panel shows post-flare eruptions approximately 2 hr before the CME. Though it is difficult to correctly identify the eruption that led to the CME on July 7, it is clear from these images that enough activity was present during the hours leading up to the CME that this event should not be labeled as stealth.

Prominences are low-ionization and dense features above the solar surface that exist between magnetic regions of opposite polarity and appear as dark lines (called filaments) when seen on the solar disk. Twenty-two of the events analyzed in this study were associated with eruptions or partial eruptions of filaments. Figure 5 is an example of a CME that was clearly seen in LASCO C2 images on February 22 beginning at 12:48 UT and had an equally identifiable LCS. A filament eruption was clearly seen rising and disappearing in *SDO* 171 and 304 Å images. It was a rising prominence given the complexity of the structures seen in 304 Å (see the online animated version

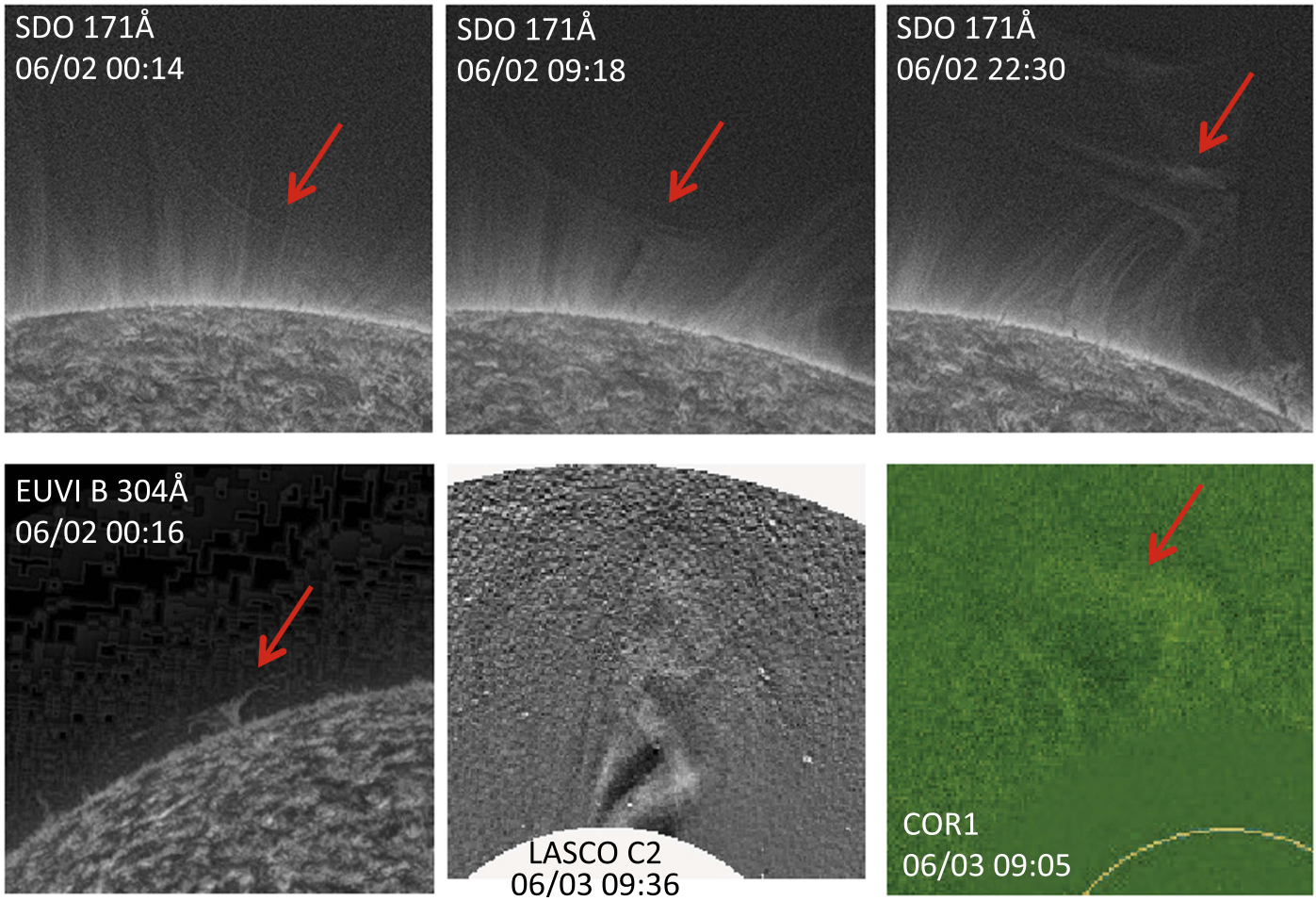

Figure 8. Event 16, which took place on June 3 beginning at 07:12 UT (seen in LASCO C2; bottom middle), was associated with a filament eruption seen in *SDO* 171 Å images (top row). Around 22:30 UT on June 2, the shape of the LCS corresponds to the shape seen in LASCO C2. In the EUVI B 304 Å image (bottom left), a prominence (indicated by the arrow) is seen at 00:16 UT. Some time later, this prominence reshapes and rises until the filament erupts leading to the CME. It is seen (faintly) in COR1 at 09:03 UT (bottom right; image credit: stereo-ssc.nascom.nasa.gov).

of Figure 5). Although this event was faint, the CME had a clear flux-tube appearance in LASCO C2, commonly associated with the eruption of a filament/cavity system (i.e., a large flux tube; Hutton & Morgan 2015). In EUV images, the source of the CME was a filament-cavity system that was slowly rising, forming the distinct flux-tube appearance of the CME in LASCO C2. The associated cavity system (the flux tube) remained at a large height for an extended period of time prior to eruption and was therefore low-density and faint. The velocity for this event in LASCO is 51 km s^{-1}, which indicates that the filament should start detaching approximately 13–14 hr before the onset of the CME in LASCO. The middle panels show the filament when it rises and reshapes in the *SDO* FOV. Prior to this, the filament is seen off limb for a long time. As it begins to rise late on February 21, it reshapes, then continues to rise until it detaches (best seen in *SDO* 304 Å, bottom right panel). Among the 22 events associated with filament eruptions in this study, we found a few with jets and small flares erupting in the vicinity of these filaments. Details are provided in Table 1.

We also looked at the filament eruption/CME pairs over the pole for further interpretation. Figure 6 shows four of these events. There was a clear LCS of an erupting filament, albeit very wispy, for events 30 and 35. Event 30 is seen expanding through the LASCO C2 FOV around 04:00 UT on October 21 (onset around 23:48 UT on October 20). The erupting filament associated with this CME is best seen in AIA 171 Å (top right). There is no evidence of an eruption in 304 Å so there is no low coronal filament eruption in the traditional sense. However, the flux tube attached above the filament definitely erupts, the helical structure of which seems to unravel during eruption. Similarly, event 35 is a beautiful eruption that behaves in the same way. Seen in LASCO C2 late on November 25, the CME is the result of a filament eruption seen in AIA 171 Å (second row, right). Based on the calculated velocity, the onset of the LCS for this event is at the beginning of November 25 (image shown here is a few hours later to show expansion).

The LCS associated with event 25 was a more obvious eruption over the north leading up to a clear CME in LASCO. The CME is shown covering the LASCO C2 FOV at 20:24 UT on August 12. There is no evidence of a large flux tube, but the LCS associated with this event is quite clearly a filament eruption. On August 11, there is a sizable filament eruption over the north, followed by smaller filament eruptions. Based on the calculated velocity, the eruption associated with this event occurs early on August 12 (shown here at 06:36 UT). Similarly, event 33 (shown in LASCO C2 at 05:48 UT on November 14) was caused by a filament eruption, though the source is likely an eruption associated with that filament. In AIA 304 Å images, jet-like eruptions occurred near the limb

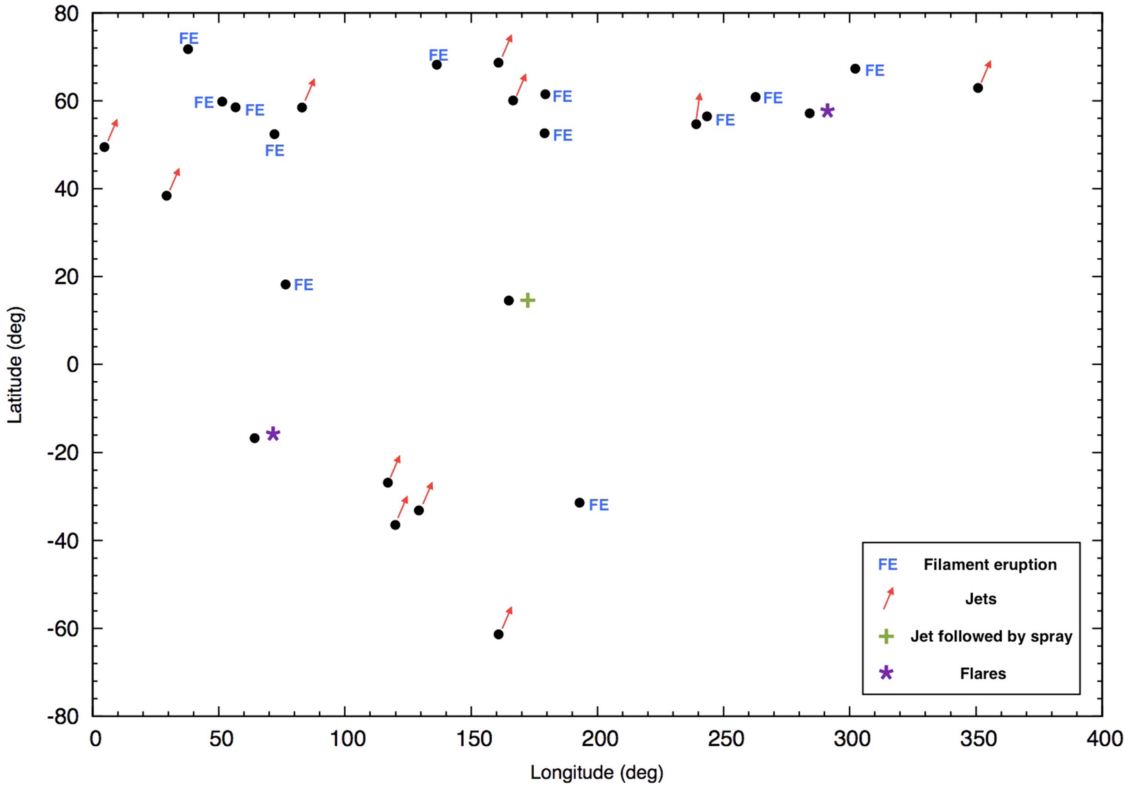

Figure 9. 3D location for most events in this study. Latitude and longitude were calculated using ACT (Hutton & Morgan 2016). The labels for each point correspond to the low coronal signature of a specific event listed in Table 1.

where the filament was located. It was very difficult to make out any obvious eruption in AIA 171 Å images.

3.1. Genuine Stealth Events?

In this study, two of the 22 LASCO events (event 12 and 16) associated with filament eruptions behaved differently in the low corona (i.e., the LCS is quite different from a typical filament eruption). Figures 7 and 8 give examples of these filament eruptions occurring at heights of about 0.1 to 0.2 $R_{\odot}$. Event 12, seen in LASCO on February 29, was a decent-sized flux-tube-like CME with no clear signature at the surface of the Sun (see Figure 7). This CME is a streamer-blowout-type CME. Streamer blowout CMEs, first described by Sheeley et al. (1982), are a subclass of CMEs that have an effect on coronal streamers. The signature of its eruption in EUV images was only a change of structure at the limit of the FOV. Some of this change in structure occurred during its eruption as seen in LASCO C2. Rather than seeing an LCS leading to an event in LASCO, we saw the eruption in LASCO C2 and viewed the consequent changes at the bottom edge of the eruption in AIA and EUVI data. Therefore, we believe that it was a flux tube that existed for a long time prior to a disruption high in the corona. When this system erupted, the observable LCS using current instrumentation was the deformation and evolution of the magnetic field lines at the base of the cavity system, as shown in the EUV images. It was possible to see the lowest part of the flux tube in some of the 171 Å images near the edge of the FOV. The large wispy structure that led to the CME was seen from the side in EUVI B and from the front in AIA 171 Å only. The same structure is also seen in SWAP (top right) but with little detail beyond what we see in AIA and EUVI. In the LASCO C2 images, the structure brightened at its position (low in the FOV) for some time before erupting. Based on qualitative analysis of the CME in LASCO, its slow appearance and eruption, its position, and the timings, this event was associated with the structure seen in the EUV images. Any other CMEs at similar positions in LASCO can be associated with other filament eruptions ruling them out, thus making this event the closest we find to a genuine stealth CME.

Figure 8 is another clear example of these high flux tubes. There is cool material condensing, collecting at the bottom, and falling down toward the Sun. Additionally, for this June 3 event, a prominence is seen in EUVI 304 Å images, which results in an eruption some time later and leads to the CME seen in LASCO C2. As previously stated, SWAP images offer a wider FOV but the low resolution makes it difficult to discern faint structures high up in the corona. The CME is faintly seen in COR1 difference images (bottom right). COR1 data would be useful to search for large flux tubes. Unfortunately, COR1 images are too noisy to show much detail.

3.2. Physical Properties

The plot in Figure 9 provides information on the distribution of LCSs for most of the events. The position of each event was calculated using the technique described in Hutton & Morgan (2016), which detects CMEs in 3D using multiviewpoint observations. Each CME signal is isolated in three coronagraph images (from *STEREO A* and *B*, and LASCO) over a sliding five-hour window using DST and intensity thresholding. Using the pixels seen to contain a CME signal between 4.5 and 5.5 $R_{\odot}$, their positions are back-projected along the line of sight. Where the back-projections intersect for the three coronagraphs is the most likely region through which the CME passed. The center of each region is found by

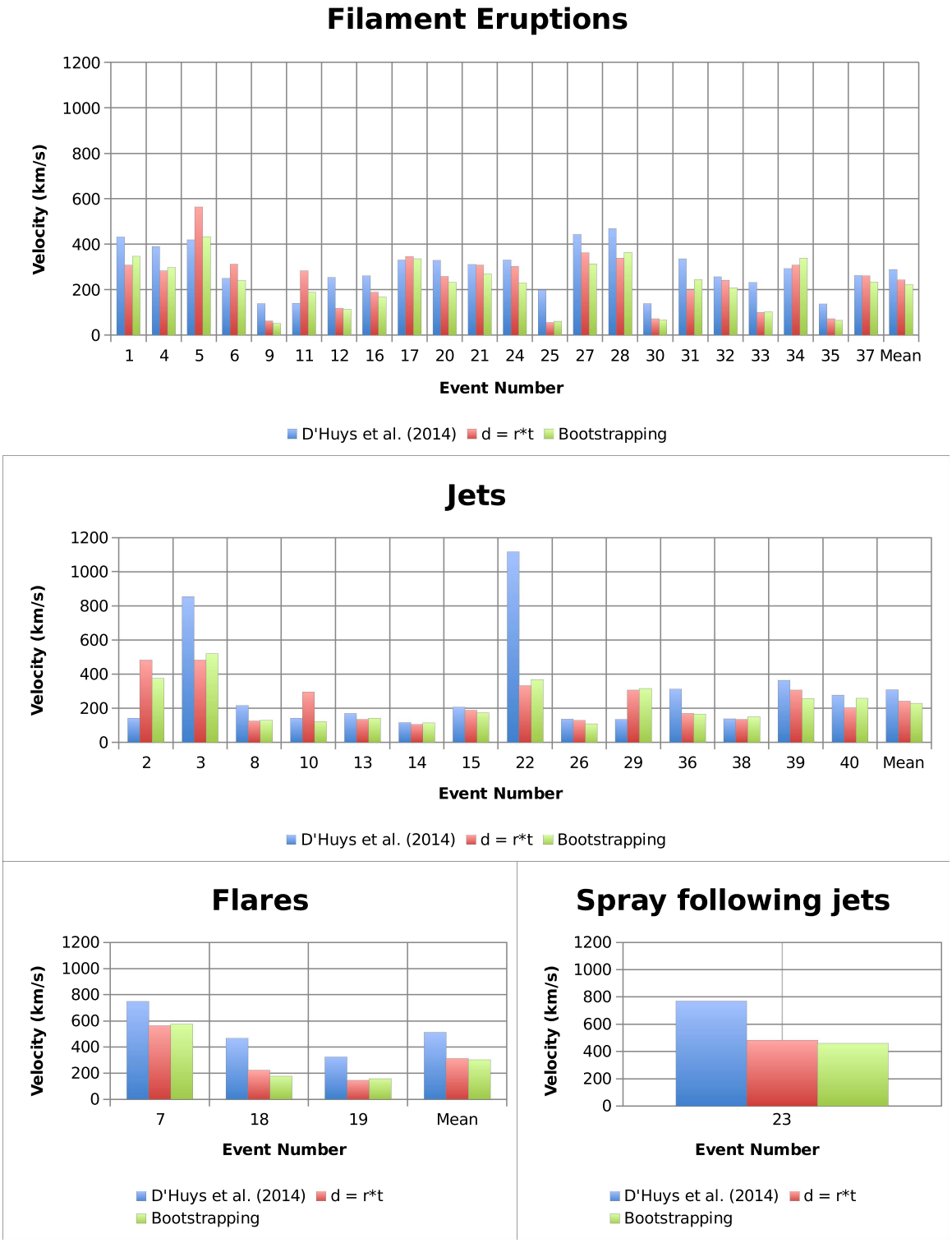

Figure 10. Velocities calculated by D'Huys (blue), by $d = rt$ (red), and by bootstrapping (green).

averaging the position of all the pixels in that signal region. Due to the faintness of many events, only 27 out of the 40 events are included in the plot, each indicated by a dot. Each dot is labeled by the LCS corresponding to that particular event. Of the 27 events shown, 12 are associated with filament eruptions, 10 of which occur above 20°. A total of 11 events are associated with jets, 7 of which occur in the region above 40°, while the remaining 4 occur between −20° and −60°.

The preponderance of events in high latitudes is possibly due to increased solar activity in the north during the rise to solar maximum. Throughout 2011 and the start of 2012, there are far more active regions in the north than in the south. As the active regions decay, their enhanced magnetic field (and increased temperature and mass) is carried slowly northward from mid-latitudes to high latitudes by meridional flows. This is a slow process taking several months. Therefore, we see in 2012 the

aftereffects of this slow dissipation. This effect is less in lower latitudes because there were far fewer active regions in the south during 2011.

The bar graphs in Figure 10 represent three different sets of velocities calculated for each of the 40 events. We used a manual "point-n-click" approach to track the heights of the leading edges of each event through the FOV of LASCO C2. From this, we created a height-time profile for each event. The linear speed and acceleration were calculated from the LASCO C2 data using a bootstrapping scheme described by Byrne et al. (2013) for a linear fit ("Linear speed") and a second-order fit (giving acceleration). The bootstrapping scheme was applied to the height-time measurements from the point-n-click procedure. The resulting speeds are represented with green bars on the graph. We also calculated the speed using the relation $d = rt$ (shown in red). These two results were then compared to the speeds calculated by D'Huys et al. (2014) under a radial assumption as well (shown in blue). Though there is a discrepancy between their results and ours, almost all velocities are of the same order of magnitude. The average speed for D'Huys et al. (2014) is approximately $324\,\mathrm{km\,s^{-1}}$ while our averages are approximately $254\,\mathrm{km\,s^{-1}}$ for $d = rt$ and approximately $236\,\mathrm{km\,s^{-1}}$ for bootstrapping.

The differences in velocities may be attributed to differences in the number of measurements taken for each event and for different time frames because this may affect the fitted function. An error is also introduced if different parts of the eruption are measured (e.g., leading edge versus cavity). One other factor that may account for the discrepancy in speeds is in the data used. The study by D'Huys et al. (2014) is based on CACTus LASCO images, which are time differenced images. The LASCO images in our study are DST-processed. One disadvantage in using time differencing is that this method may create unwanted structures that may be mistaken for coronal transients. Additionally, the quiescent coronal structure changes brightness considerably so any long-term time differencing will result in an unwanted brightness signal (Morgan et al. 2012). For a few events, events 3 and 22, in particular, there is a large discrepancy in velocity. For event 3, we measured a blob that entered the LASCO C2 FOV in the aftermath of a large CME. It is possible that different transients were measured between the two studies. The discrepancy in the velocities for event 22 is unclear and requires further analysis.

4. Summary and Conclusions

The term "stealth" CME was first coined by Robbrecht et al. (2009b) to draw attention to the fact that some low-latitude (possibly geo-effective) CMEs were only first detected in coronagraph data several hours after an initial eruption (their LCS was impossible to view against the disk in EUV), and therefore they would be difficult to detect in a future early forecast system. In addition to the work by D'Huys et al. (2014), other studies such as Kilpua et al. (2014), Ma et al. (2010), and Wang et al. (2011) have identified CMEs as stealth. Vourlidas et al. (2011) describe their stealth event as having "very weak low corona signatures as viewed from Earth." All of these studies emphasize the difficulty in observing LCSs. Wang et al. (2011) go further by stating that the LCSs of these events are not visible in EUV pass-bands and, sometimes, not visible in coronagraphs facing them (i.e., halo CMEs). Howard & Harrison (2013) argue that stealth CMEs are classified as such based on observations, stating that correct identification of these events is limited by instrument sensitivity and bandwidth issues. It follows then that the dynamics of faint LCSs are often missed because of limitations in instruments and image processing. The image processing techniques used in our study of stealth CMEs are essential in revealing the hard-to-observe signatures of these events, thus confirming the conclusions reached in previous works.

The lack of observable evidence of LCSs can be taken to mean that there are no LCSs, or that there is some unknown, new class of difficult-to-observe LCS. In this sense, some eruptions of high-latitude and high-altitude filament-cavity systems fit this latter interpretation. However, all 40 events studied here possess some form of LCS. Through careful processing of EUV images using the new state-of-the-art image processing techniques, we were able to show LCSs that led to ejections previously referred to as stealth CMEs. We found that most of the events in this study are small unstructured blobs or puffs, often occurring in the aftermath of a large CME. Their inclusion in previous studies may be due to the use of output from an automated CME catalog.

Based on our analysis of all 40 events, we are in agreement with the conclusions of Robbrecht et al. (2009b) and D'Huys et al. (2014) that LCSs of stealth CMEs are very faint events that form higher in the corona or in low-density regions of magnetic field weaker than usual CME-forming regions (i.e., filament eruptions or active regions). Additionally, our study of the 40 CME events previously studied by D'Huys et al. (2014) reveals that each one has an on-disk (or off-limb) signature association. A stealth CME is therefore a misconception arising from observational and processing limitations.

N.A. acknowledges the valuable discussions and insights provided by Shadia Habbal during this study. She is grateful to Elke D'Huys for discussing her 2014 study of these events. H.M. is grateful for funding from the Leverhulme Foundation that made his contribution to this paper possible. The *SDO* data used are provided courtesy of NASA/*SDO* and the AIA science team. The *STEREO*/SECCHI project is an international consortium of the Naval Research Laboratory (USA), Lockheed Martin Solar and Astrophysics Lab (USA), NASA Goddard Space Flight Center (USA), Rutherford Appleton Laboratory (UK), University of Birmingham (UK), Max-Planck-Institut für Sonnen-systemforschung (Germany), Centre Spatial de Liege (Belgium), Institut d'Optique Théorique et Appliquée (France), and Institut d'Astrophysique Spatiale (France).

References

Alzate, N., & Morgan, H. 2016, ApJ, 823, 129
Bonte, K., Berghmans, D., De Groof, A., Steed, K., & Poedts, S. 2013, SoPh, 286, 185
Brueckner, G. E., Howard, R. A., Koomen, M. J., et al. 1995, SoPh, 162, 357
Byrne, J. P., Long, D. M., Gallagher, P. T., et al. 2013, A&A, 557, A96
Chen, P. F. 2011, LRSP, 8, 1
D'Huys, E., Seaton, D. B., Poedts, S., & Berghmans, D. 2014, ApJ, 795, 49
Halain, J.-P., Berghmans, D., Seaton, D. B., et al. 2013, SoPh, 286, 67
Hanser, F. A., & Sellers, F. B. 1996, Proc. SPIE, 2812, 344
Howard, R. A., Sheeley, N. R., Jr., Koomen, M. J., & Michels, D. J. 1985, JGR, 90, 8173
Howard, R. A., Moses, J. D., Vourlidas, A., et al. 2008, SSRv, 136, 67
Howard, T. A., & Harrison, R. A. 2013, SoPh, 285, 269
Hutton, J., & Morgan, H. 2015, ApJ, 813, 35
Hutton, J., & Morgan, H. 2016, A&A, 599, A68
Kilpua, E. K. J., Mierla, M., Zhukov, A. N., et al. 2014, SoPh, 289, 3773
Lemen, J. R., Title, A. M., Akin, D. J., et al. 2012, SoPh, 275, 17

Ma, S, Attrill, G. D. R., Golub, L., & Lin, J. 2010, ApJ, 722, 289
Morgan, H. 2015, ApJS, 219, 23
Morgan, H., Byrne, J. P., & Habbal, S. R. 2012, ApJ, 752, 144
Morgan, H., & Druckmüller, M. 2014, SoPh, 289, 2945
Morgan, H., Habbal, S. R., & Woo, R. 2006, SoPh, 236, 263
Robbrecht, E., & Berghmans, D. 2004, A&A, 425, 1097
Robbrecht, E., Berghmans, D., & Van der Linden, R. A. M. 2009a, ApJ, 691, 1222
Robbrecht, E., Patsourakos, S., & Vourlidas, A. 2009b, ApJ, 701, 283
Schanche, N. E., Reeves, K. K., & Webb, D. F. 2016, ApJ, 831, 47
Seaton, D. B., Berghmans, D., Nicula, B., et al. 2013, SoPh, 286, 43
Sheeley, N. R., Howard, R. A., Koomen, M. J., et al. 1982, SSRv, 33, 219
Vourlidas, A., Colaninno, R., Nieves-Chinchilla, T., & Stenborg, G. 2011, ApJL, 733, L23
Vourlidas, A., Lynch, B. J., Howard, R. A., & Li, Y. 2013, SoPh, 284, 179
Wang, Y., Chen, C., Gui, B., et al. 2011, JGR, 116, A04104